# Supporting Information

Kueh *et al.* 10.1073/pnas.0807394105

## SI Text

**Note 1.** Although hard to precisely quantify, the slow pointed end shrinkage rate was significantly larger than zero in our experiment, which we determined by comparison to shrinkage rates of filaments elongating in unlabeled actin monomer (Fig. S1). In all of our experiments there also existed a small subpopulation with shrinkage rates that appeared indistinguishable from zero (not shown in Fig. 1*F* and shown in red in Fig. S1*C*), suggesting that there may also exist multiple dynamic states at the pointed end. However, the slow rate of pointed end shrinkage precluded imaging observation of transitions between these possible states.

**Note 2.** Our experimental setup was optimized to minimize possible interactions between actin filaments and the imaging environment. Perfusion chambers were blocked extensively by using casein and nonionic detergents. Moreover, filamin concentrations were chosen to attach filaments to the chamber at only a few points, giving rise to filaments that fluctuated considerably in the imaging plane. Under such conditions, we observed filaments that did not shrink even though both ends were fluctuating freely. Conversely, there were shrinking filaments that depolymerized past a filamin attachment point without stopping. Although these observations do not rule out stabilizing interactions between immobilized filaments and their immediate environment, they do suggest that filament immobilization alone does not sufficiently explain the existence of a slow-shrinking filament population in our imaging assays.

**Note 3.** A single exponential fitted the data poorly (data not shown), consistent with the notion that a single shrinkage rate does not adequately explain our observations, as previously noted (1, 2). Exponential decay of pyrene signal is expected for endwise depolymerization at a constant rate, because spontaneously nucleated filaments show an exponential length distribution (3).

**Note 4.** The same result was noted when the filaments were bundled during depolymerization (Fig. S3), implying that filament bundling had little effect on filament depolymerization or stabilization in this assay.

**Note 5.** Similar rate increases were obtained by using a kymograph analysis of selected filaments (Fig. S6). We also note that Andrianantoandro *et al.* (4) observed a decrease in the rate of barbed end filament shrinkage in the presence of cofilin. The discrepancy between their study and ours may arise because of differences in filament age, immobilization conditions, and/or cofilin concentrations used.

**SI Results.** ***Filaments switch to a stable slow-shrinking state in solution.*** The persistent pyrene signal due to F-actin may reflect the existence of a stable slow-shrinking filament population, as suggested by imaging observations. Alternatively, it may simply reflect a sharp decrease in the number of filament ends over time, possibly due to complete depolymerization of short filaments or end-to-end filament annealing. To distinguish between these alternative possibilities, we repeated the above experiment with fluorescently labeled actin, polymerizing Alexa Fluor 647-labeled actin filaments in solution for 1 h and then adding LatB to remove free monomer. At different times during the reaction, filaments in solution were attached to filamin-coated perfusion chambers and imaged by using time-lapse microscopy (Fig. S2*A*). When filaments were imaged immediately before LatB addition, they showed two distinct rates of filament shrinkage, with 45% of the imaged filaments existing in a slow-shrinking state (Fig. S2*B*, black bar). Consistent with these observations, the histogram of shrinkage rates exhibited revealed two dynamically distinct populations (Fig. S2*C*). When filaments were imaged 1 or 3.5 h after LatB addition, they also showed two dynamically distinct rates of depolymerization; however, the fraction of slow-shrinking filaments increased significantly to 75% and 78% at 1 and 3.5 h after LatB addition, respectively (Fig. S2*B*, red bars). We also repeated this experiment using DNase I and vitamin D-binding protein (DBP), two proteins that also sequester free monomer. Incubation with DNase I or DBP for 1 or 3.5 h also significantly increased the fraction of stable slow-shrinking filaments (Fig. S2*B*, green and blue bars), arguing that our results reflect a consequence of monomer removal and not simply an unwanted effect of LatB. The shrinkage rate histogram for filaments treated with DBP for 3.5 h also exhibited two dynamically distinct filament populations (Fig. S2*D*). Whereas the mean shrinkage rates for both populations were similar to those before DBP treatment, the relative sizes of the both populations had changed substantially, with an increase in the size of the slow-shrinking population and a concomitant decrease in the size of the fast-shrinking population (Fig. S2 *C* and *D*). In contrast, we did not observe an increase in the mean filament length after monomer sequestration (Fig. S2*E*), arguing that our pyrene data (Fig. 2*A*) cannot be explained by elimination of short filaments or filament annealing. These results argue that the persistent pyrene signal observed after monomer removal (Fig. 2*A*) does not arise from a decrease in the number of filament ends; instead, it arises because filaments switch from a dynamic fast-shrinking state to a stable slow-shrinking state as they age, even when diffusing in solution.

***Aged filaments are more susceptible to cofilin-mediated severing.*** We here determine how filament age affects filament severing by cofilin. Previous studies have suggested that cofilin promotes rapid actin turnover by severing filaments (5, 6), although we have argued that bursting from filament ends, which also requires Aip1 and coronin, may be more relevant in cells (7). We compared the severing of new (3 min old) and aged (25 min old) filaments treated with 8 $\mu$M cofilin. Remarkably, when newly polymerized filaments were perfused with cofilin, hardly any severing occurred initially; 100 s after the onset of imaging, only 2% of all visible filaments severed (Fig. S5, top, $n = 405$). In contrast, when filaments were first aged in buffer for 25 min and then perfused with 8 $\mu$M cofilin, they severed extensively, with 29% of all filaments visibly breaking within 100 s (Fig. S5, red carets, $n = 288$). These results suggest that aged filaments are much more susceptible than young filaments to severing by cofilin.

Why does cofilin preferentially severs aged actin filaments? One obvious possibility is that differences in nucleotide content between new and aged filaments may render these two populations differentially susceptible to cofilin-mediated severing. As cofilin binds to ADP-F-actin with higher affinity than ATP-F-actin (8), it is plausible that cofilin does not bind to and sever young filaments ($\approx$3 min in age) because they have not yet released their bound $\gamma$-phosphate ($P_i$) and thus contain mainly ATP or ADP-$P_i$ (9, 10). However, given evidence that cofilin accelerates $\gamma$-$P_i$ release from actin filaments (11), it is also possible that young filaments treated with cofilin have released a large fraction of their inorganic phosphate.

An alternative possibility is that different susceptibilities of new and aged filaments to severing may stem from differences in

filament internal structure between these two populations. When cofilin binds to an aged Holmes-like filament, it may induce subunits in its neighborhood to adopt a "tilted" state and create an interface between "tilted" and Holmes-like subunits within a single filament. As recently proposed, such interfaces between different structural states may be energetically unfavorable and hence especially susceptible to breakage (6). Because many young filaments already exist in a cofilin-induced "tilted" state (12), they may not accumulate similar structural heterogeneities within a single filament upon cofilin binding and may therefore be less susceptible to breakage.

Regardless of underlying cause, the finding that cofilin does not sever young filaments that are ≈3 min in age compels us to reexamine the role of severing in rapid actin turnover in vivo. Dynamic actin assemblies in cells and organisms turn over with a half-life of <60 s (13, 14). As filaments in these assemblies are nucleated and depolymerized within this timescale, they may not survive long enough to undergo the age-dependent changes that render them susceptible to severing by cofilin. Thus, we think that rapid turnover of filaments in these dynamic assemblies cannot be catalyzed by cofilin-mediated severing and must instead occur through alternative pathways. It is still unclear how cofilin promotes turnover of dynamic actin assemblies in cells and organisms. Recent work in our laboratory has shown that rapid actin disassembly requires other biochemical factors in addition to cofilin (15). This full purified system can catalyze the rapid depolymerization of young actin filaments (7) and may hence be relevant for studying mechanisms of rapid actin disassembly in physiological settings.

***Nonmuscle actin filaments also stabilize with age.*** All experiments in the main text were performed with actin purified from rabbit skeletal muscle (16), which is relatively inert to depolymerization in the muscle cell. To determine whether age-dependent filament stabilization also occurs with an actin that is more dynamic in a physiological context, we purified nonmuscle actin from bovine calf thymus, which expresses exclusively nonmuscle isoforms of actin ($\beta$- and $\gamma$-actin) (17). As determined by filament elongation off *Limulus* acrosomal bundles (18), purified thymus actin exhibited a barbed-end elongation rate, $k_b$, and critical concentration, $[C_c]$, similar to those of skeletal muscle actin (Fig. S7*A*), consistent with published comparative studies (19). We next performed single-filament imaging, as per Fig. 1. Time-lapse movies of newly polymerized single thymus actin filaments revealed two dynamically distinct filament populations with vastly different population kinetics (Fig. S7 *B–E*). Similar to skeletal muscle actin, the fraction of stable filaments increased with filament age and reached an asymptote smaller than unity (Fig. S7*F*). The fraction of stable filaments present in young thymus actin was higher than that present in young skeletal muscle actin. The reason behind this difference is unclear. Nonetheless, our results support the idea that, similar to skeletal muscle actin, thymus actin also forms filaments that stabilize with age. Interestingly, the shrinkage rates observed for thymus actin filaments were substantially higher than those for skeletal muscle actin (Fig. S7 *B–E*). As revealed by a double-Gaussian fit to the shrinkage rate histogram (Fig. S7*G*, black curve), the dynamic population of filaments depolymerized at a mean rate of 6.4 subunits per second, whereas the stable population depolymerized at a mean rate of 0.3 subunits per second. Both rates were ≈3-fold higher than those observed for the corresponding dynamic (1.8 subunits per second) and stable (0.1 subunits per second) filament populations observed in skeletal muscle actin (Fig. 1*F*).

**SI Materials and Methods.** ***Imaging of filaments aged in bulk solution.*** For imaging of actin filaments polymerized/depolymerized in bulk solution, filaments were polymerized in solution by incubating 3 $\mu$M Alexa Fluor 647 actin monomer in assay buffer for 1 h. Polymerized filaments were then either imaged directly or treated with LatB, DNase I, or DBP prior for varying amounts of time before imaging. To immobilize filaments for imaging, the actin filament solution was perfused into filamin-coated perfusion chambers. To minimize filament shearing, wide-mouth pipette tips were used for pipetting F-actin solutions. After a sufficient number of immobilized filaments had attached to the coverslip for imaging (typically requiring 1–3 min of incubation), unattached filaments and unpolymerized monomer were then washed out with assay buffer containing oxygen scavengers and 10% blocking solution. To ensure that filaments under different conditions received equal times of exposure to the perfusion chamber surface, time-lapse imaging was initiated exactly 4 min after the perfusion of the actin filament solution in all experiments. Time-lapse images were then segmented and analyzed as described above.

***Gel filtration of unlabeled actin monomer.*** Skeletal muscle actin was purified by using two polymerization/depolymerization cycles, as described in the main text. Purified actin monomer was then loaded onto a Superdex 200 gel filtration column (300 mL total volume) equilibrated with buffer A (2 mM Tris·Cl/0.2 mM $CaCl_2$/0.2 mM ATP/ 0.1% 2-mercaptoethanol/0.005% $NaN_3$, pH 8.0). The actin monomer eluted as a single symmetric peak at from 150–170 mL, as detected by absorbance at 280 nm. A fraction from the trailing edge of this peak was taken for subsequent polymerization/depolymerization assays.

***Imaging of filaments elongated from* Limulus *acrosomal bundles.*** A procedure similar to that described in the main text was followed for all experiments in Figs. S3. S4, and S7, with the following modifications: For experiments in Fig. S3, *Limulus* acrosomal fragments were first labeled with by incubation with 3 $\mu$M TRITC-phalloidin for 3 min (P1951; Sigma), washed, then incubated with 3 $\mu$M gel-filtered actin monomer for 7 min. Filaments were depolymerized in buffer alone for varying times, stabilized with 3 $\mu$M FITC-phalloidin (P5282; Sigma) for 3 min, washed, perfused with filamin, and imaged. For experiments in Fig. S4, filaments elongated from *Limulus* acrosomal fragments were bundled with filamin, then allowed to depolymerize in buffer during time-lapse acquisition. For experiments in Fig. S7, *Limulus* acrosomal bundles with incubated with either Alexa Fluor 647-labeled rabbit skeletal muscle actin or Alexa Fluor 647-labeled calf thymus actin for varying times. Immediately after polymerization, filaments were washed, bundled, and stabilized by using 5 $\mu$M phalloidin and 50 mM spermidine in assay buffer, then imaged.

***Purification of actin from bovine calf thymus.*** Nonmuscle actin was purified from bovine calf thymus by using a combination of methods described in refs. 16 and 20. Ten grams of bovine calf thymus acetone powder (57052; Pel-Freez Biologicals) was extracted with 200 mL G buffer with 1 mM PMSF for 30 min and clarified by centrifugation at 140,000 × *g* for 1 h (*k*-factor = 220) at 4 °C. The clarified supernatant was then filtered and loaded onto a 100-mL DEAE-cellulose (D3764; Sigma) anion exchange column equilibrated with G buffer plus 100 mM KCl and presaturated with ATP. The DEAE column was then washed with 300 mL of G buffer plus 100 mM KCl and eluted with a 1,200-mL gradient to 500 mM KCl in G buffer. Actin-containing fractions, which eluted between 150 and 250 mM KCl, were then pooled and polymerized by addition of 2 mM $MgCl_2$ followed by incubation at 25 °C for 1 h. Polymerized actin was pelleted by centrifugation at 26,000 × *g* at 4 °C for 13 h (*k*-factor = 1,200) and subject to a depolymerization/polymerization cycle. This procedure yielded 70 mg of nonmuscle actin as determined by a Bradford assay (note that optimal conditions for protein storage have not yet been determined). The actin was then labeled on lysines by using Alexa Fluor 647 NHS-ester and converted to Ca-G-ATP before imaging, as described above.

1. Walsh TP, Weber A, Higgins J, Bonder EM, Mooseker MS (1984) Effect of villin on the kinetics of actin polymerization. *Biochemistry* 23:2613–2621.
2. Bryan J, Coluccio LM (1985) Kinetic analysis of F-actin depolymerization in the presence of platelet gelsolin and gelsolin-actin complexes. *J Cell Biol* 101:1236–1244.
3. Kawamura M, Maruyama K (1972) A further study of electron microscopic particle length of F-actin polymerized in vitro. *J Biochem* 72:179–188.
4. Andrianantoandro E, Pollard TD (2006) Mechanism of actin filament turnover by severing and nucleation at different concentrations of ADF/cofilin. *Mol Cell* 24:13–23.
5. Maciver SK, Zot HG, Pollard TD (1991) Characterization of actin filament severing by actophorin from *Acanthamoeba castellanii*. *J Cell Biol* 115:1611–1620.
6. Andrianantoandro E, Pollard TD (2006) Mechanism of actin filament turnover by severing and nucleation at different concentrations of ADF/cofilin. *Mol Cell* 24:13–23.
7. Kueh HY, Mitchison TJ, Brieher WM (2008) Actin filament disassembly by cofilin, coronin, and Aip1 occurs in bursts and is inhibited by barbed-end cappers. *J Cell Biol* 182:341–353.
8. Carlier MF, *et al.* (1997) Actin depolymerizing factor (ADF/cofilin) enhances the rate of filament turnover: Implication in actin-based motility. *J Cell Biol* 136:1307–1322.
9. Melki R, Fievez S, Carlier MF (1996) Continuous monitoring of Pi release following nucleotide hydrolysis in actin or tubulin assembly using 2-amino-6-mercapto-7-methylpurine ribonucleoside and purine-nucleoside phosphorylase as an enzyme-linked assay. *Biochemistry* 35:12038–12045.
10. Carlier MF, Pantaloni D (1986) Direct evidence for ADP-Pi-F-actin as the major intermediate in ATP-actin polymerization. Rate of dissociation of Pi from actin filaments. *Biochemistry* 25:7789–7792.
11. Blanchoin L, Pollard TD (1999) Mechanism of interaction of Acanthamoeba actophorin (ADF/Cofilin) with actin filaments. *J Biol Chem* 274:15538–15546.
12. Orlova A, *et al.* (2004) Actin-destabilizing factors disrupt filaments by means of a time reversal of polymerization. *Proc Natl Acad Sci USA* 101:17664–17668.
13. Theriot JA, Mitchison TJ (1991) Actin microfilament dynamics in locomoting cells. *Nature* 352:126–131.
14. Wang YL (1985) Exchange of actin subunits at the leading edge of living fibroblasts: Possible role of treadmilling. *J Cell Biol* 101:597–602.
15. Brieher WM, Kueh HY, Ballif BA, Mitchison TJ (2006) Rapid actin monomer-insensitive depolymerization of Listeria actin comet tails by cofilin, coronin, and Aip1. *J Cell Biol* 175:315–324.
16. Pardee JD, Spudich JA (1982) Purification of muscle actin. *Methods Enzymol* 85:164–181.
17. Su AI, *et al.* (2002) Large-scale analysis of the human and mouse transcriptomes. *Proc Natl Acad Sci USA* 99:4465–4470.
18. Pollard TD (1986) Rate constants for the reactions of ATP- and ADP-actin with the ends of actin filaments. *J Cell Biol* 103:2747–2754.
19. Gordon DJ, Boyer JL, Korn ED (1977) Comparative biochemistry of non-muscle actins. *J Biol Chem* 252:8300–8309.
20. Gordon DJ, Eisenberg E, Korn ED (1976) Characterization of cytoplasmic actin isolated from Acanthamoeba castellanii by a new method. *J Biol Chem* 251:4778–4786.

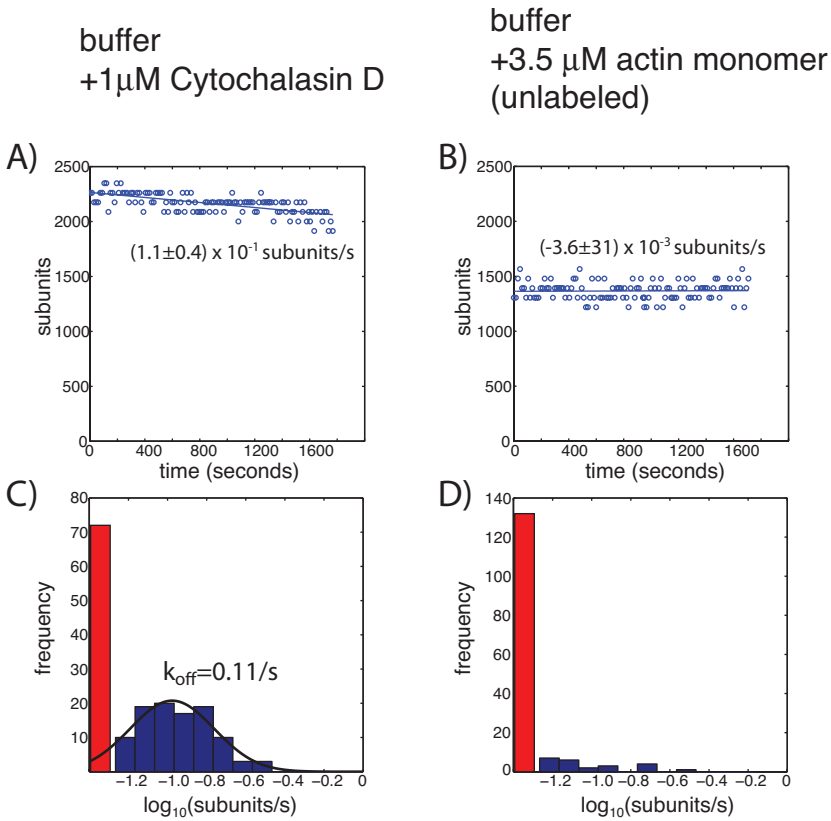


**Fig. S1.** The stable filament population shrinks slowly from pointed ends at a non-zero rate. Shown are length versus time traces for representative single actin filaments in buffer and 1 $\mu$M CytoD (*A*) or in buffer and 3.5 $\mu$M unlabeled actin monomer (*B*). Straight lines represent best linear fits to the data, and rate constants give the shrinkage rate at its 95% confidence bound as determined from the linear fit. Also shown are shrinkage rate histograms for actin filaments in buffer and 1 $\mu$M CytoD (*C*) or in buffer and 3.5 $\mu$M unlabeled actin monomer (*D*). A red bar denotes the filament subpopulation that shortened by $<$1 pixel during the entire time-lapse movie and has $k_{off} < 0.043$ subunits per second. This subpopulation was enriched in filaments incubated with unlabeled monomer (85%, $n = 155$) compared with filaments incubated with 1 $\mu$M CytoD (46%, $n = 173$, $\chi^2 = 119$, $P < 0.01$). Single Gaussian fit to the shrinking filament subpopulation (smooth black curve) gives a mean shrinkage rate of 0.11 subunits per second.

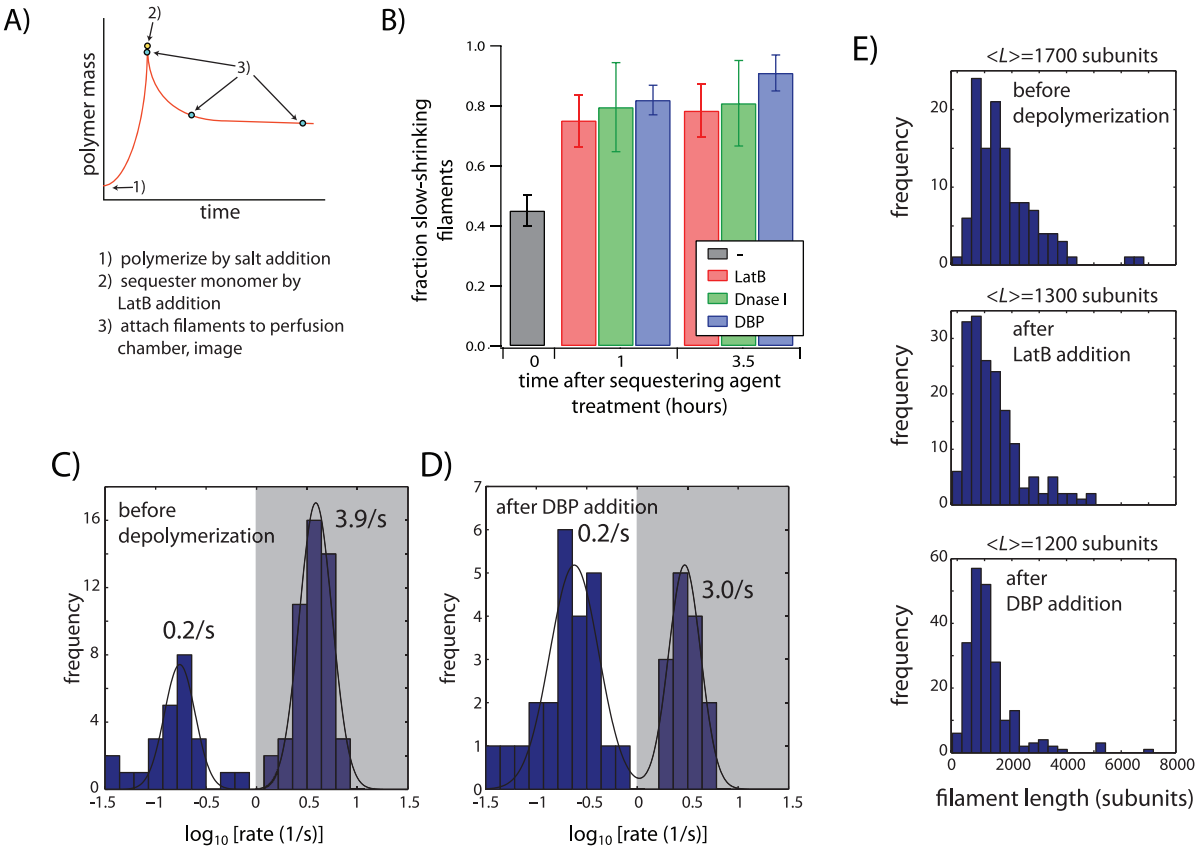


**Fig. S2.** The slow phase of depolymerization observed in bulk assays reflects switching of filaments to a slow-shrinking state. (*A*) Description of the experiment, showing correspondence with Fig. 2*A*. (*B*) Bar chart showing fraction of slow-shrinking filaments in a population of Alexa Fluor 647 actin filaments that had been polymerized in solution for 1 h and then imaged directly (black bar) or treated with 12 $\mu$M LatB (red bars), 12 $\mu$M DNase I (green bars), or 12 $\mu$M DBP (blue bars) for the indicated time before imaging. Data represent mean and SD of 3 independent experiments. (*C*) Histogram of shrinkage rates for filaments imaged before addition of monomer-sequestering agent. (*D*) Histogram of shrinkage rates for filaments imaged 3.5 h after DBP addition. (*E*) Length distributions for filaments immediately before monomer sequestering agent agent (*Top*), 3.5 h after LatB addition (*Middle*), and 3.5 h after DBP addition (*Bottom*). Mean filament lengths $\langle L \rangle$ in subunits are given on the top of each graph.

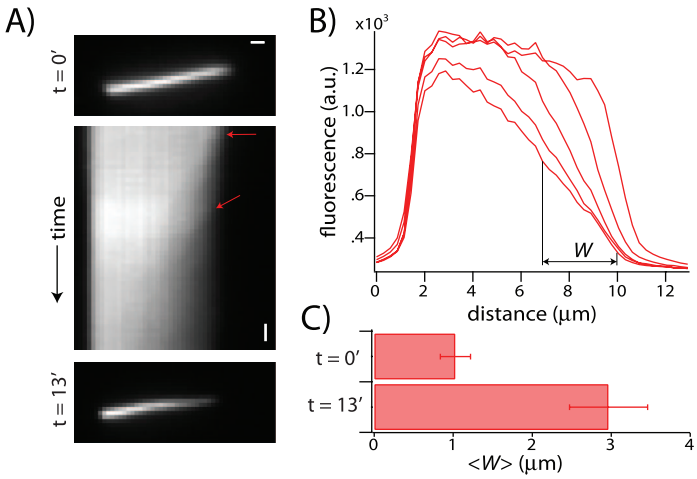


**Fig. S3.** Depolymerization and stabilization of filamin-bundled actin filaments. (*A*) Time-lapse images of actin filaments elongated from a single *Limulus* acrosomal fragment, bundled by using filamin, and then depolymerized in buffer. Images were taken immediately at the onset of imaging (*Top*) and 13 min later (*Bottom*). Filament barbed ends are oriented toward the right. (Scale bar: 1 $\mu$m.) Kymograph (*Middle*) shows fluorescence intensity along the filament bundle contour over time. (Scale bar: 1 min.) The diagonal lines along the kymograph reflect the presence of filament shrinkage in the bundle (red arrows). Kymograph analysis of filament shrinkage rates revealed a mean shrinkage rate of 3.2 $\pm$ 0.3 subunits per second ($n$ = 13). (*B*) Line scans along the contour of the same filament bundle, taken, from right to left, 0, 3, 5, 8, and 10 min after the onset of time-lapse imaging. *W* denotes the half-width of intensity drop at the barbed end. (*C*) Mean half-width of the intensity drop at the barbed end, $\langle W \rangle$, taken at the onset of imaging (*Upper*) and 13 min later (*Lower*). Data represent mean and SD of 12 filament bundles from 2 experiments. A comparison of these images and line scans with those from Fig. 3 shows that filamin bundling does not strongly affect the kinetics of filament depolymerization and stabilization.

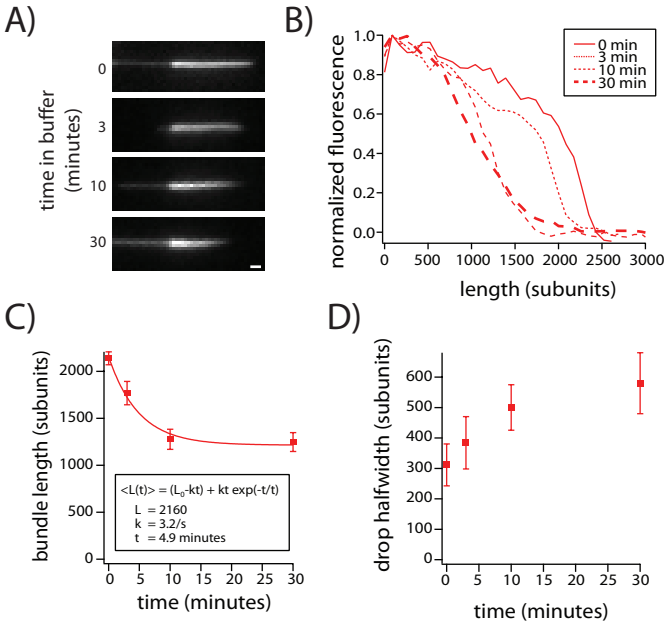


**Fig. S4.** Actin purified by gel filtration also stabilizes with age. (*A*) Images of actin filament bundles polymerized from *Limulus* acrosomal fragments by using gel-filtered monomer, depolymerized by monomer washout, then fixed and stained by using rhodamine-phalloidin at different times after the start of depolymerization. (Scale bar: 1 $\mu$m.) (*B*) Fluorescence intensity line scans along the contour of the filament bundles shown in *A*. Line scans are normalized so that the maximal fluorescence value is set to unity and the minimal fluorescence value is set to zero. (*C*) Graph showing filament bundle length as a function of time of depolymerization. Bundle length was measured from line scans as the distance from the base of the acrosomal bundle to the point where actin fluorescence intensity dropped to half of its maximal value. Data represent mean and SD of 12 filament bundles. Smooth curve represents fit of the data to a simple model, where filaments with starting length *L* depolymerize at a constant rate *k*, then switch to a nonshrinking state with first order rate *r*. The equation in the *Inset* gives the time evolution of the mean filament length as predicted by this model. Data represent mean and SD of 12 filament bundles. The values below give the best fits values for *L*, *r*, and *k*. These values are consistent with those reported in Fig. 1. (*D*) Graph showing half-width of the intensity drop at the barbed end as a function of depolymerization time. The magnitude of the increase ($\approx$300 subunits) is more consistent with that expected from the simple two-state model ($\sim kr/2 \approx$ 500 subunits) and less consistent with the filaments shrinking at a constant rate [$\sim$(subunits depolymerized)$^{1/2} \approx$ 30 subunits)].

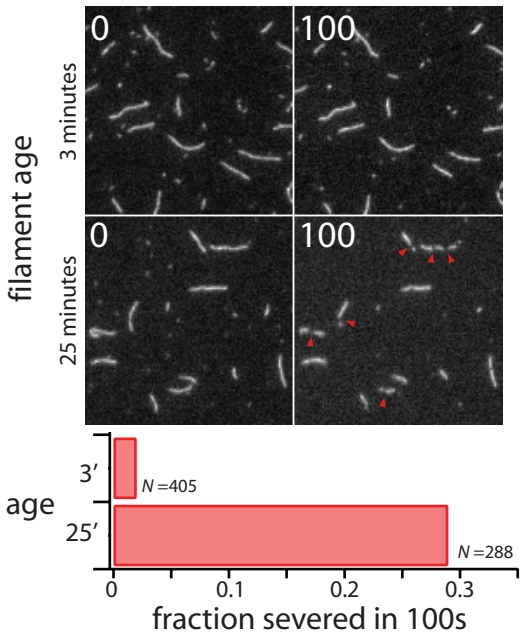


**Fig. S5.** Aged filaments are more susceptible to cofilin-mediated severing. Newly polymerized filaments (3′, *Upper*) or aged filaments (25′, *Lower*) were treated with 8 $\mu$M cofilin. Time-lapse images were taken either zero seconds (*Left*) or 100 seconds after start of imaging after cofilin perfusion. Severing events are denoted by red arrowheads. The bar chart compares fraction of newly polymerized filaments to fraction of aged filaments that severed within 100 s after cofilin treatment.

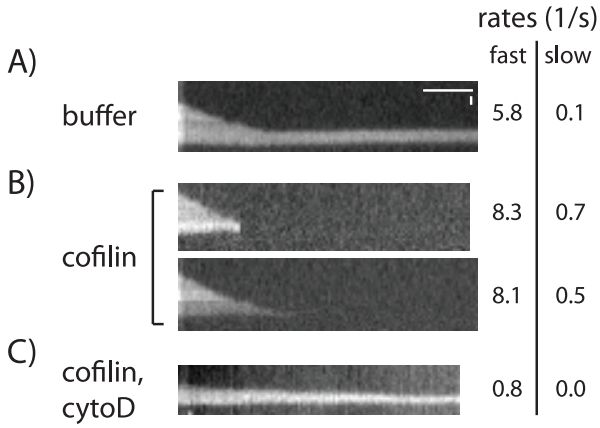


D)

| | shrinkage rate (subunits/s) | |
|---|---|---|
| | more dynamic end | less dynamic end |
| **buffer** ***(N=11)*** | 4.8±1.2 | 0.18±0.14 |
| **cofilin** ***(N=10)*** | 7.8±4.2 | 0.79±0.41 |
| **cofilin+CytoD** ***(N=13)*** | 0.88±0.49 | 0.023±0.058 |

**Fig. S6.** Kymograph analysis of aged filaments treated with cofilin (from experiments shown in Fig. 3). Kymographs show an aged filament in buffer (*A*), two aged filaments in cofilin (*B*), and an aged filament in cofilin and CytoD (*C*). (Vertical scale bar: 1 $\mu$m experiments shown in Horizontal scale bar: 100 s.) Numbers to the right give shrinkage rates for the shown kymographs at the more dynamic end (fast) and at the less dynamic end (slow), determined by measuring the angle of straight lines manually drawn at both filament ends on the kymograph. (*D*) Table showing the mean and standard deviation for shrinkage rates under different conditions, as determined by kymograph analysis.

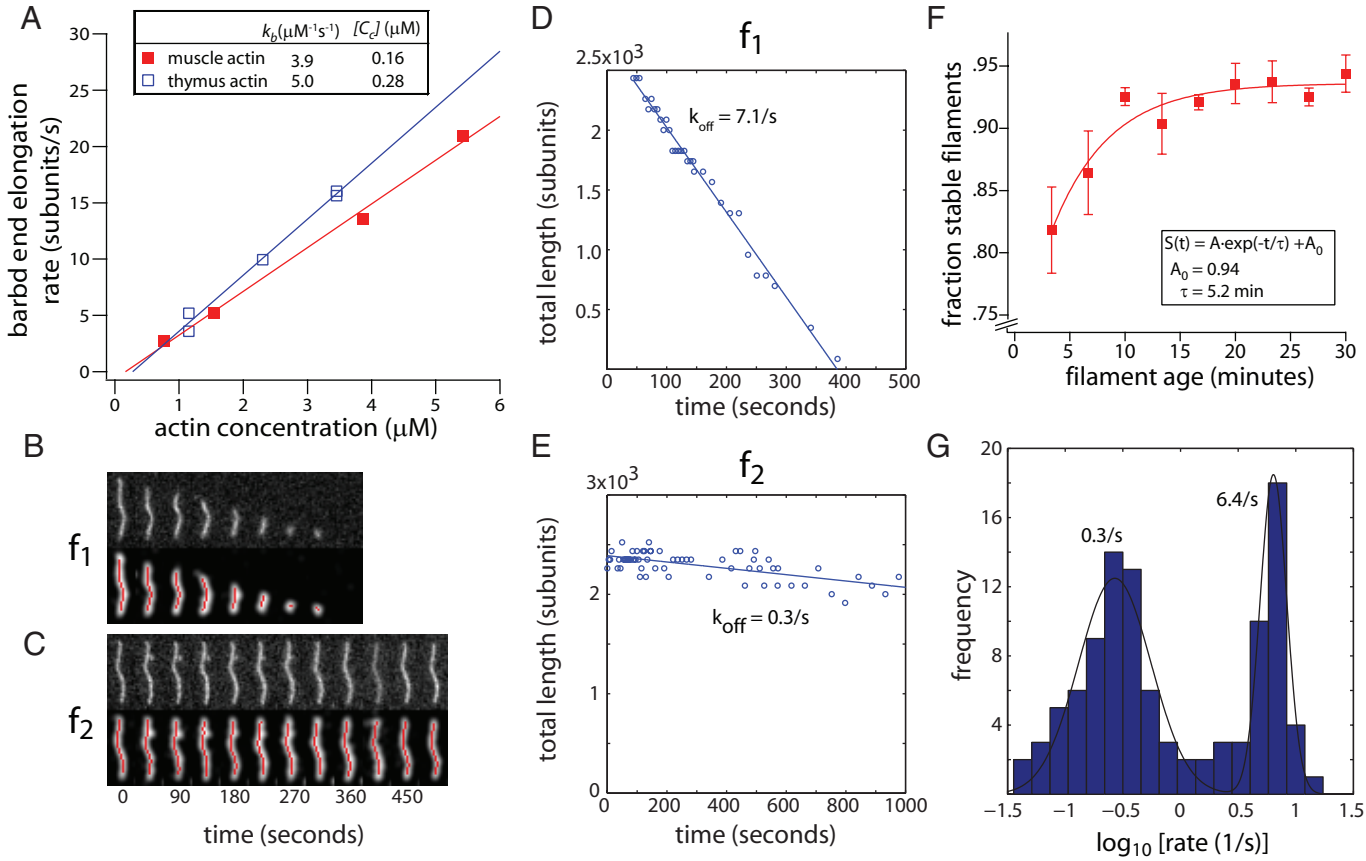


**Fig. S7.** Nonmuscle actin filaments also stabilize with age. (*A*) Graph of barbed-end elongation rate as a function of actin concentration for muscle actin (red) and nonmuscle actin (blue), obtained by measuring filament bundle growth off *Limulus* acrosomal process fragments. Best linear fits to the data, shown by the straight lines, give the elongation rate $k_b$ and critical concentration [$C_c$]. (*B* and *C*) Successive time-lapse images of a dynamic fast-shrinking filament, $f_1$ (*B*), and a static slow-shrinking filament, $f_2$ (*C*). (*D* and *E*) A plot of the total lengths of $f_1$ and $f_2$ as a function of time, as well as best linear fits to the data (straight lines). (*F*) Fraction of stable nonshrinking filaments as a function of filament age, given by time elapsed after initiation of polymerization (red squares). Data represent mean and SD of 3 independent experiments. Smooth curve shows fit of the data to a single exponential $S(t) = A\exp(-t/\tau) + A_0$. (*G*) Histogram of filament shrinkage rates (blue), shown on a log scale. A two-component Gaussian fit to the shrinkage rate histogram (smooth black curve) gives mean shrinkage rates for the fast-shrinking and slow-shrinking filament populations of 6.4 subunits per second and 0.3 subunits per second, respectively.

**Table S1. Shrinkage rates under different conditions**

| Condition | Mean shrinkage rate, subunits/s (SD of Gaussian fit) | |
|---|---|---|
| | Fast | Slow |
| 1 min of polymerization, imaged in buffer alone | 1.8 (1.1–2.8) | 0.14 (0.07–0.25) |
| 1 min of polymerization, imaged in 1 $\mu$M CytoD | — | 0.11 (0.08–0.37) |
| 1 h of polymerization, imaged in buffer alone | 3.9 (2.3–6.6) | 0.17 (0.13–0.24) |
| 1 h of polymerization, 3.5 h of DBP incubation, imaged in buffer alone | 3.0 (1.8–4.9) | 0.24 (0.11–0.52) |
| 1 min of polymerization, 30 min of buffer incubation, imaged in buffer alone | 2.7 (1.6–4.5) | 0.11 (0.04–0.33) |
| 1 min of polymerization, 30 min of buffer incubation, imaged in 4 $\mu$M cofilin | 5.9 (3.1–11.4) | 0.79 (0.45–1.4) |
| 1 min of polymerization, 30 min of buffer incubation, imaged in 4 $\mu$M cofilin and 1 $\mu$M CytoD | — | 1.1 (0.7–1.9) |
| 1 min of polymerization (nonmuscle actin), imaged in buffer alone | 6.4 (4.4–9.3) | 0.27 (0.09–0.75) |